Showcasing research from Professor Byun's laboratory, Department of Mechanical Engineering, Sungkyunkwan University, Suwon, South Korea; Professor Lee's laboratory, Department of Materials Science and Engineering, Pusan National University, Busan, South Korea; and Professor Cho's laboratory, School of Mechatronics Engineering, Gyeongsang National University, Jinju, South Korea

Strain-induced electrification-based flexible nanogenerator for efficient harvesting from ultralow-frequency vibration energy at 0.5–0.01 Hz

The demand for edge computing and next-generation devices has increased the need for self-powered sensors, especially in biomedical and wearable tech. Nanogenerators, like triboelectric nanogenerators (TENGs), show promise, but efficient power generation at ultralow frequencies (<0.1 Hz) is challenging. This study introduces a strain-induced electrification-based nanogenerator (SIE-NG) that efficiently generates power at 0.01 Hz with a current density of 2.3 mA m^{-2}. SIE-NG avoids repetitive contact processes, ensuring stable output even after 1×10^6 cycles, offering a breakthrough for wearable and biomedical applications.

As featured in:

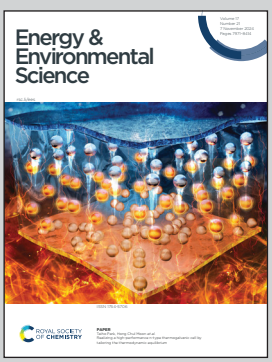

See Doyoung Byun, Dae-Hyun Cho *et al.*, *Energy Environ. Sci.*, 2024, **17**, 8111.

ROYAL SOCIETY OF CHEMISTRY

rsc.li/ees

Registered charity number: 207890

Energy & Environmental Science

ROYAL SOCIETY OF CHEMISTRY

PAPER

View Article Online
View Journal | View Issue

Cite this: *Energy Environ. Sci.*, 2024, **17**, 8111

Strain-induced electrification-based flexible nanogenerator for efficient harvesting from ultralow-frequency vibration energy at 0.5–0.01 Hz†

Joonkyeong Moon,‡[a] Seoung-Ki Lee,‡[b] Busi Im,[a] Doyoung Byun*[a] and Dae-Hyun Cho*[cd]

The demand for self-powered devices, particularly in biomedical and wearable technology, emphasizes efficient powering from ultralow-frequency vibrations. While triboelectric nanogenerators have shown potential, they still face challenges in powering below 0.1 Hz and suffer from tribological issues. Herein, we introduce a novel nanogenerator capitalizing the strain-dependent characteristics of the work function of gold. Our device achieves efficient power generation at 0.01 Hz, with a current density of 2.3 mA m^{-2}, marking a significant breakthrough. At 0.5 Hz, it reaches 4.8 mA m^{-2}, demonstrating substantial improvement over prior performance. Moreover, by eliminating repetitive contact-separation processes found in triboelectric nanogenerators, our generator exhibits no performance degradation due to tribological damage after 1 000 000 cycles. Integrated into a watch strap, it powers LEDs and generates Morse code signals *via* finger grasping, offering an innovative method for distress communication when conventional power sources are unavailable. The wide material selectivity for strain-modifiable work functions suggests promising research avenues.

Received 22nd May 2024,
Accepted 14th August 2024

DOI: 10.1039/d4ee02225d

rsc.li/ees

Broader context

The increasing demand for self-powered devices, particularly in biomedical engineering and wearable technology, highlights the necessity for efficient energy harvesting from ultralow-frequency vibrations. Although triboelectric nanogenerators provide promise, they struggle to generate power below 0.1 Hz and have tribological issues. To address these limitations, we developed a flexible nanogenerator exploiting the strain-dependent characteristics of the gold's work function. By capitalizing on the charge-transfer mechanism between the gold and dielectric layers, our nanogenerator achieves efficient power generation even at frequencies as low as 0.01 Hz, with a maximum current density of 2.3 mA m^{-2}. This is a significant breakthrough, as no previous reports have achieved power generation at this ultralow frequency. At 0.5 Hz, our nanogenerator achieves 4.8 mA m^{-2}, signifying a substantial improvement over prior performance levels. Furthermore, our nanogenerator eliminates the need for repetitive contact-separation processes inherent in conventional triboelectric nanogenerators, exhibiting no performance degradation after 1 000 000 cycles. Integrated into a watch strap, the nanogenerator successfully illuminates light-emitting diodes, and generates an S.O.S signal in Morse code even under slow finger grasping below 0.2 Hz, highlighting advantages for wearable and biomedical applications. The wide selectivity for materials whose work functions can be modified by strain presents promising avenues for future research.

Introduction

The increasing demand for edge computing technology and the synergistic effect of enabling devices with various form factors have increased the demand for next-generation standalone devices. In particular, to satisfy the requirements of power efficiency and autonomy for sensor components that acquire data from the external environment, nanogenerators with integrated sensing and self-powering capabilities are preferred over conventional setups that combine sensor devices with distinct energy-storage units.[1,2] Therefore, studies pertaining to self-sustaining sensor devices that utilize nanogenerators

[a] *Department of Mechanical Engineering, Sungkyunkwan University, Suwon 16419, Republic of Korea. E-mail: mjk4304@skku.edu*
[b] *School of Materials Science and Engineering, Pusan National University, Busan 46241, Republic of Korea*
[c] *Department of Mechatronics Engineering, Gyeongsang National University, Jinju 52725, Gyeongnam, Republic of Korea*
[d] *Department of Energy System Engineering, Gyeongsang National University, Jinju 52828, Gyeongnam, Republic of Korea*

† Electronic supplementary information (ESI) available: Methods, Fig. S1–S3, Tables S1–S9, and Supplementary Videos. See DOI: https://doi.org/10.1039/d4ee02225d

‡ These authors contributed equally to this work.

based on electromagnetic,[3] electrostatic,[4] triboelectric,[5] and piezoelectric[6] effects are actively being conducted in diverse scientific domains. However, despite the potential of nanogenerators, ongoing refinements are needed to ensure efficient and reliable power generation at low trigger frequencies. Since the rate of change in the electric field induced by mechanical vibration critically determines the output performance of nanogenerators, the current technology remains insufficient to yield adequate power for practical applications.[7] In the emerging field of biomedical engineering, most of the mechanical energy generated by the human body during daily activities operates at frequencies below 1 Hz. Ultralow-frequency mechanical inputs, from the gentle rhythm of breathing (<0.4 Hz) to the subtle motions of various activities,[8] including the heartbeat (~ 0.1 Hz),[9] are significant.[10] In the analysis of cardiovascular interactions, such as respiration, heart rate variability, and systolic blood pressure, biosignals below 0.1 Hz are important.[11,12] Therefore, to develop sophisticated biomedical applications, improving the operating frequency limits of nanogenerators to capture and utilize these ultralow frequencies is imperative.[13,14]

Among the various types of nanogenerator devices, the triboelectric nanogenerator (TENG) exhibits superior performance, even at low frequencies.[7,15] Jung *et al.* designed a cylindrical-type TENG with magnets to store potential energy, which achieved an average power density of 0.49 W m^{-3} at a frequency of 0.33 Hz.[16] Y. Peng *et al.* fabricated a soft-contact cylindrical TENG with an average power density of 0.23 W m^{-3} at a frequency of 0.1 Hz.[17] Despite efforts to reduce the operating frequency with these approaches, rigid and bulky structures are unsuitable for biomedical and wearable devices. Consequently, the focus has shifted to flexible and compact TENGs, which have promise for biomedical and wearable applications. However, the current technological limit for average power density at a frequency of 0.5 Hz is 0.75 W m^{-2}.[18] Notably, studies on the effective power generation below 0.1 Hz in biomedical and wearable applications have not been performed, as evidenced by the literature.

Researchers have recently focused on mitigating friction and the durability challenge in TENGs caused by friction and wear by exploring solutions using solid or liquid lubricants such as diamond-like coatings,[19] nanocomposite materials,[20] and greases.[21] Solid lubricants have the potential to prolong TENG lifespan by reducing interfacial wear, but selecting suitable materials poses challenges due to factors like dielectric constants and thermal stability. Additionally, in cases where the contact is nonconformal, output loss occurs due to air breakdown.[22] Liquid lubricants, although a viable approach, can complicate the design of TENGs, thus rendering them less suitable for biomedical or wearable device applications, where simplicity and miniaturization are essential.[23] Another alternative is noncontact TENGs, which inherently eliminate friction and wear.[24] However, they are typically limited in terms of power generation; thus, they are more suitable for sensor applications than self-powering systems.

To address the low-frequency powering and tribological issues presented by nanogenerators, this study introduces a novel strain-induced electrification-based nanogenerator (SIE-NG). The operating principle of the nanogenerator is based on the charge-transfer mechanism of conventional TENGs, which is driven by the equilibrium tendency of the surface potential between the contacting materials.[24] However, SIE-NG does not require repetitive mechanical contact processes because it utilizes strain-induced modulation of the work function for energy conversion. Specifically, the developed nanogenerator utilizes strain-induced electrification as the primary driving mechanism instead of conventional contact electrification, which occurs *via* contact between two active layers. Utilizing this unique method of power generation, SIE-NG achieves efficient power generation even at frequencies as low as 0.01 Hz, with a maximum current density of 2.3 mA m^{-2}. This is a significant breakthrough, as no previous reports have achieved power generation at this ultralow frequency. At 0.5 Hz, SIE-NG achieves a high current density exceeding 4.8 mA m^{-2}; this value is almost twice the previously reported highest value.[25] Notably, SIE-NG is composed of an ultra-thin structure that includes a layer of gold (Au), which is known for its significant work-function variation under strain, and a double layer of relatively stable polyethylene terephthalate (PET).[26] Moreover, since the repetitive contact-separation processes at the Au/PET interface is not required, SIE-NG is not affected by the performance degradation typically associated with wear and chemical deterioration, thus maintaining a stable output even after 1 000 000 cycles. This groundbreaking approach provides new opportunities for practical applications in biomedical engineering, wearable technology, and other domains, thereby addressing critical issues in the field of nanogenerators.

Results and discussion

Operation mechanisms of strain-induced electrification

In contact electrification as typical operation mechanism, when two materials with differing electronegativities establish contact with each other, electrons hop over a potential barrier, which is denoted by W herein. Fig. 1(a) shows a conceptual diagram of the contact electrification between an insulator and a metal. Here, E_n and * represent the neutral level of the surface state in the dielectric and the energy level at the interface under the equilibrium state, respectively. A material possessing a higher work function tends to acquire electrons and becomes negatively charged, whereas a material with a lower work function behaves oppositely to achieve a balanced surface potential between the materials.[27] From an electromagnetic perspective, the height of the barrier (W) represents the potential difference between the two materials ($|\text{W.F.} - E_n|$), where W.F. refers to the work function. Additionally, from a morphological perspective, inherent surface roughness creates an unavoidable air gap during contact. This gap acts as an additional barrier ($\Delta E_{\text{air gap}}$), lowering charge transfer efficiency.[28]

Conversely, strain-induced electrification occurs at the interface where a metal and an insulator are in direct contact, each exhibiting significantly different responses to strain-induced change in their work functions. The equilibrium states of the

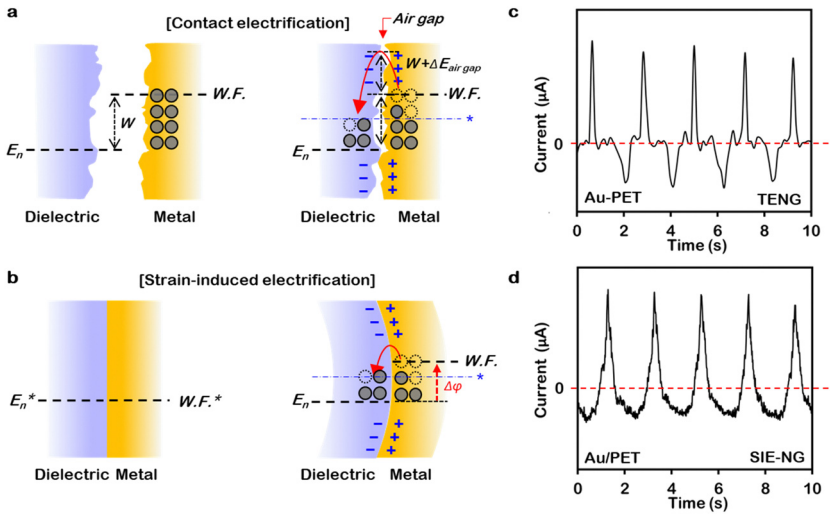

Fig. 1 Surface-state diagram illustrating the electrification of the dielectric–metal interface, which indicates charge transfer between the dielectric and metal: (a) contact electrification when two materials with differing electronegativities establish contact with each other; (b) strain-induced electrification while the surface potential is adjusted under a material-modified work function; this is considerably affected by mechanical strain by bending. (c) and (d) Instantaneous short-circuit current of (c) contact electrification and (d) strain-induced electrification; E_n, neutral level of the surface state in the dielectric; * energy level at the interface under equilibrium.

dielectric (E_n*) and metal layers (W.F.*) may be disrupted when mechanical strain is applied to adjacent materials. This disruption is caused by the correlation between the mechanical strain and the work function of the materials, as depicted in Fig. 1(b). Specifically, if the work function of one of the materials (*e.g.*, a metal) is altered significantly by the mechanical strain and that of the other material (*e.g.*, a dielectric) remains relatively unchanged, then electron transfer inevitably occurs to balance the surface potential in response to the work-function changes induced by the mechanical strain. Additionally, the metal layer, deposited on the insulator using the thermal evaporation method, effectively eliminates air gaps, thereby maximizing the efficiency of electron hopping at the interface.

To substantiate this hypothesis, Au, which is characterized by a significant variation in the work function relative to strain, and copper (Cu), which is not, were selected as the metal layers based on a literature review.[26,29] PET is a representative plastic substrate and known for its minimal alteration in work function under strain;[30] thus, PET was used as both the counter material and substrate. Upon mechanical bending, the 40-nm-thick Au/PET double layer generated a distinct voltage oscillation that was easily distinguishable from the noise, as shown in Supplementary Video 1 (ESI†); this video shows the real-time output voltage generated by the bending the Au/PET double layer, and the results are consistent with our assumptions. However, when the 40-nm-thick Cu/PET double layer was bent, as shown in Supplementary Video 2 (ESI†), no output signal was generated. The occurrence of localized stress gradients during bending tests necessitates the consideration of flexoelectricity in the insulating substrate.[31] However, experimental results for the Cu/PET double layer indicate that its flexoelectric effect is undetectable and does not significantly influence the overall output of the proposed mechanism we suggested. Therefore, our hypothesis that the change in work function due to strain is the driving force behind electric output generation is supported by the conclusions from these data. Due to a different electrification mechanism, the SIE-NG exhibits different output signals from the TENGs upon contact with and separation from the Au-PET as shown in Fig. 1(c) and (d).

Further examination of the proposed power generation mechanism indicated that alterations in the work function of the Au layer induced by mechanical deformation could significantly affect the intensity of the output power. The initial step involved quantifying the change in the work function of the Au layer under applied mechanical strain. Kim *et al.* demonstrated that the elastic limits of Au films with thicknesses of 55, 85, and 400 nm were less than 0.25%, as determined *via* tensile tests conducted on water surfaces.[32] Similarly, M. A. Haque and M. T. A. Saif identified elastic limits below 0.25% for 200- and 350-nm-thick Au films *via* microtensile tests performed on free-standing films.[33] Based on these studies, we targeted work-function variations under uniaxial strains of 0%, 0.11%, 0.15%, and 0.18%, focusing on elastic strain effects (Fig. S1, ESI†). This approach considers only reversible effects from elastic deformation relevant to nanogenerators or sensors operating under continuous vibrations. Fig. 2 shows the ultraviolet photoelectron spectroscopy (UPS) spectra and the shift in the work function of the Au layers with tensile strain. The work function of the flat Au layer was measured to be 4.98 eV, which was consistent with the general value of Au.[34] As the tensile strain increased to 0.18%, the work function reduced to 3.98 eV, which is consistent with reported data from 20-nm-thick Au ($\partial E/\partial\varepsilon = -1.83$ V)[26] and *ab initio* calculation result ($\partial E/\partial\varepsilon = -1.89$ V).[35] It is known that the loss in electron density and the usual shrinkage of the surface dipole were caused by the

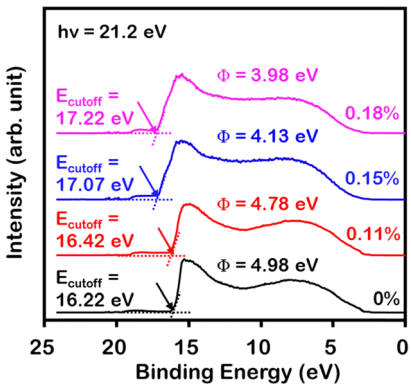

Fig. 2 UPS spectra obtained from the Au layers with tensile strains of 0%, 0.11%, 0.15%, and 0.18% and work functions calculated from the corresponding E_f, hv, and E_{cutoff}.

transverse elastic response of the lattice and functioned synergistically in a laterally tensile material to decrease the dipole strength, thus decreasing the work function.[35]

The output performance of SIE-NG at ultralow-frequencies

Fig. 3 shows the output performance of the proposed SIE-NG, which operated at a strain frequency of 0.25 Hz on various substrates with a consistent Au layer. We presumed that the performance is attributed mainly to the change in the work function of the Au layer due to tensile strain, without any triboelectric charging induced by the repetitive contact process. Similar power generation behavior has been observed for other representative flexible substrates exhibiting relatively stable work functions against strain, such as polyimide (PI) and ultrathin glass (UTG). Fig. 3(a)–(c) present the output voltages generated from the Au layers on the PET, PI, and UTG substrates, respectively (Tables S1–S3, ESI†). The strain-dependent current densities for different substrates are shown in Fig. 3(d)–(f) and Tables S1–S3 (ESI†); here, both the output voltages and current densities increased with increasing tensile strain. These results strongly support our hypothesis that the strain-dependent work function of gold, when in contact with substrates exhibiting minimal strain-dependence in work function, is the primary mechanism underlying the electric outputs generated by the SIE-NG.

However, the output performance varies slightly depending on the underlying substrate type, as depicted in Fig. 3(g) (for detailed data, see Table S4, ESI†). If the change in the work function of Au is the sole contributor to the powering performance, then the performance difference depending on the substrate type shown in Fig. 3(g) cannot be elucidated. A possible factor is the difference in the effective strain applied to the Au layer due to the different roughness degrees of the substrate.[36] It is important to note that the calculated strains presented here assume ideal flat substrates (Methods, ESI†).

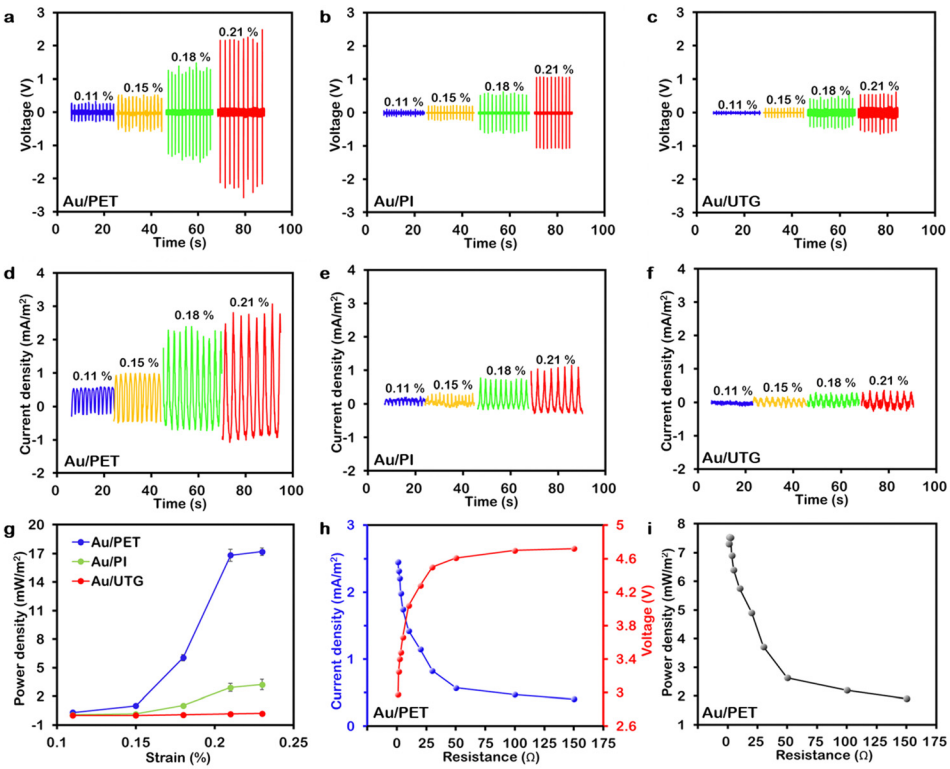

Fig. 3 Comparison of the output performances of Au/PET-, Au/PI-, and Au/UTG-based SIE-NGs at a frequency of 0.25 Hz. Effects of strain on the output voltages of (a) Au/PET, (b) Au/PI, and (c) Au/UTG. Effects of strain on the current densities of (d) Au/PET, (e) Au/PI, and (f) Au/UTG. (g) Comparison of the effects of strain on the power densities of Au/PET, Au/PI, and Au/UTG with a tensile strain of 0.21%. (h) Output current density, voltage and (i) power density of Au/PET under different external loads with a tensile strain of 0.18%.

Hence, the actual effective strain applied to the Au layer may be different if the roughness of the substrate surface is considered. As shown in Fig. S2 (ESI†), the PET, PI, and UTG substrates had different root mean square (RMS) roughness values of 97.0, 37.9, and 5.7 nm, respectively. Therefore, we inferred that a rougher substrate resulted in a larger strain compared with a smoother substrate even under the same bending radius; this may have occurred because of the strain-concentration effect, which may result in greater charge transfers and consequently higher outputs. To further investigate the effect of roughness, PET substrates with RMS roughness values of 2.01, 3.42, and 7.35 μm were prepared (Methods, ESI†), as shown in Fig. S3a (ESI†). As the RMS roughness increased, the current density of the Au layers on the polished PETs increased, as shown in Fig. S3b (ESI†); these results indicated that the surface roughness of the substrate significantly affected the SIE-NG performance. However, from the UPS results in Fig. S3c (ESI†), the changes in the work functions of the polished PET substrates with strain were negligible. This result indicates that the actual effective strain for rougher PET did not notably impact the work function of the Au layer, despite the likely higher level of effective strain. Therefore, the strain concentration effect on a rough surface could not account for the effect of substrate surface roughness. Next, we considered the effect of the real contact area between the Au layer and its substrate. According to Xu *et al.*, the larger real contact area, where triboelectrification occurs, could generate greater outputs of TENGs.[37] Similarly, the phenomenon of strain-induced electrification in SIE-NG occurred at the real contact area, namely, at the interface between the Au layer and its substrate. Since, the Au layer and its substrate likely form conformal contacts during the thermal evaporation process, accordingly, rougher substrates likely create larger interfaces with the Au layer, resulting in greater electrification and consequently higher output, as shown in Fig. 3(g) and Fig. S3b (ESI†). A peak current density of 2.32 mA m^{-2} was achieved under a load resistance of 1.5 Ω; this value corresponded to an instantaneous power density of 7.53 mW m^{-2}, as shown in Fig. 3(h), (i) and Table S5 (ESI†).

Fig. 4 shows the effect of the motion frequency on the output performance of an SIE-NG composed of Au/PET. Similar to the characterization of TENGs,[38] the output current density and voltage were measured with a tensile strain of 0.21% at different frequencies ranging from 0.01 to 0.5 Hz (Fig. 4(a), (b) and Table S6, ESI†), and the peak power density was 15 mW m^{-2} at 0.5 Hz, as shown in Fig. 4(c) and Table S6 (ESI†). In this case, the output performance decreased with the decrease in frequency, similar to the behavior observed in TENGs and PENGs.[15] Nevertheless, the SIE-NG performed better at ultralow frequencies of 1 Hz or less, as shown in Fig. 4(d). To the best of our knowledge, Wang's TENG exhibited the highest current density of 2.78 mA m^{-2} at a low operating frequency of 0.5 Hz.[25] Our proposed SIE-NG performed better by approximately two-fold at the same frequency. Moreover, compared with previously reported data[14,17,25,39–43] (Table S7, ESI†), the decrease in the performance of SIE-NG with decreasing frequency was less pronounced, as shown in Fig. 4(d). Notably, at an extremely low frequency of 0.01 Hz, where no previous data was reported, our SIE-NG achieved a current density of 2.3 mA m^{-2}, thus highlighting its superior performance at frequencies where conventional energy harvesting technologies tend to fail.

Before using a nanogenerator in practical applications, its durability needed to be tested. The Au/PET-based SIE-NG underwent rigorous bending tests simulating gentle human motion.[8] As shown in Fig. 4(e) and Table S8, (ESI†), the SIE-NG

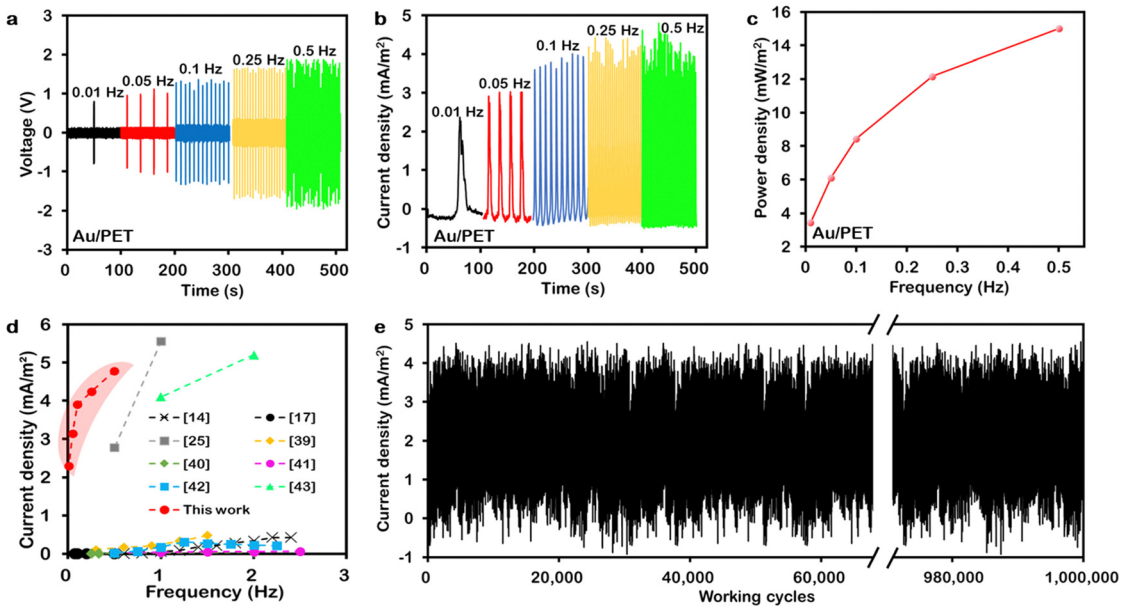

Fig. 4 Performance of the Au/PET-based SIE-NG with a tensile strain of 0.21%: (a) output voltage, (b) current density, and (c) power density at different frequencies under external load of 1.5 Ω. (d) Comparison of the current density with the reported data for the low-frequency triboelectric nanogenerators. (e) Changes in the current density during cyclic bending for up to 1 000 000 cycles at a frequency of 0.25 Hz with a tensile strain of 0.21%.

exhibited no degradation even after 1 000 000 cycles, thus demonstrating its exceptional durability. A crucial aspect of the design of the SIE-NG is the absence of tribological issues at the interface between the Au layer and PET substrate, which is critical for charge transfer. This absence increases the robustness of our device and contributes to its overall durability. Therefore, our proposed approach not only enables the harvesting of ultralow-frequency energy but also ensures the robustness of the nanogenerator, thus addressing major challenges in the field of TENGs.[1,44,45]

Application of SIE-NG as a wearable distress communication device

Fig. 5 presents the applications of the Au/PET SIE-NG as a power source for commercial light-emitting diodes (LEDs) and wearable devices. To evaluate its capability for ultralow-frequency powering, the SIE-NG was connected *via* a rectifier and capacitor circuit (Fig. 5(a)). Capacitors of 0.33, 1.00 and 2.40 μF were charged by the SIE-NG under 0.2% strain at a frequency of 0.25 Hz for 50 s (Fig. 5(b) and Table S9, ESI†). Larger capacitors exhibited lower voltages ranging from 4.6 to 0.8 V. The potential of the SIE-NG for ultralow-frequency powering was further demonstrated by its integration with a watch strap to power LEDs and generate emergency rescue signals, as shown in Fig. 5(c). The SIE-NG illuminated the five LEDs using the energy from the 2.4 μF capacitor charged *via* finger grasping (Fig. 5(d) and Supplementary Video 3, ESI†); this generated an ultralow frequency of less than 0.2 Hz. Additionally, the unique application of the SIE-NG is its integration into a watch strap, which enables the wearer to generate electricity through minimal movement. Distinct from conventional nanogenerators that primarily function as supplementary power sources to extend the battery lifespan, the SIE-NG-equipped strap provides a significant advantage: it enables individuals in distress, *i.e.*, with limited mobility, to transmit a rescue signal. As shown in Fig. 5(e) and Supplementary Video 4 (ESI†), at low frequencies below 0.5 Hz, a distinct S.O.S. signal was effectively generated by slowly clenching the fingers to bend the strap, which successfully generated Morse-code signals. This highlights the potential of the SIE-NG as a life-saving device in emergency situations, thus offering an innovative method for distress communication when conventional power sources are unavailable.

Conclusion

We introduce a groundbreaking advancement in nanogenerator technology aimed at overcoming key challenges in ultralow-frequency power generation and durability. Our innovative design of SIE-NG leverages the strain-dependent work function of Au to achieve remarkable efficiency, enabling operation at ultralow-frequency as low as 0.01 Hz with a notable current density of 2.3 mA m^{-2}, a feat unprecedented in previous reports. Additionally, at a frequency of 0.5 Hz, the device exhibited a remarkable current density of 4.8 mA m^{-2}, outperforming previously reported levels. Moreover, SIE-NG exhibits exceptional durability, exhibiting no performance degradation after 1 000 000 operating cycles. Practical demonstrations, such as the integration into a watch strap for LED illumination and Morse code signaling, highlight its potential as a power source for diverse wearable and biomedical applications. This offers an innovative method for distress communication, effective even during slow human motion. Because of the wide selectivity for

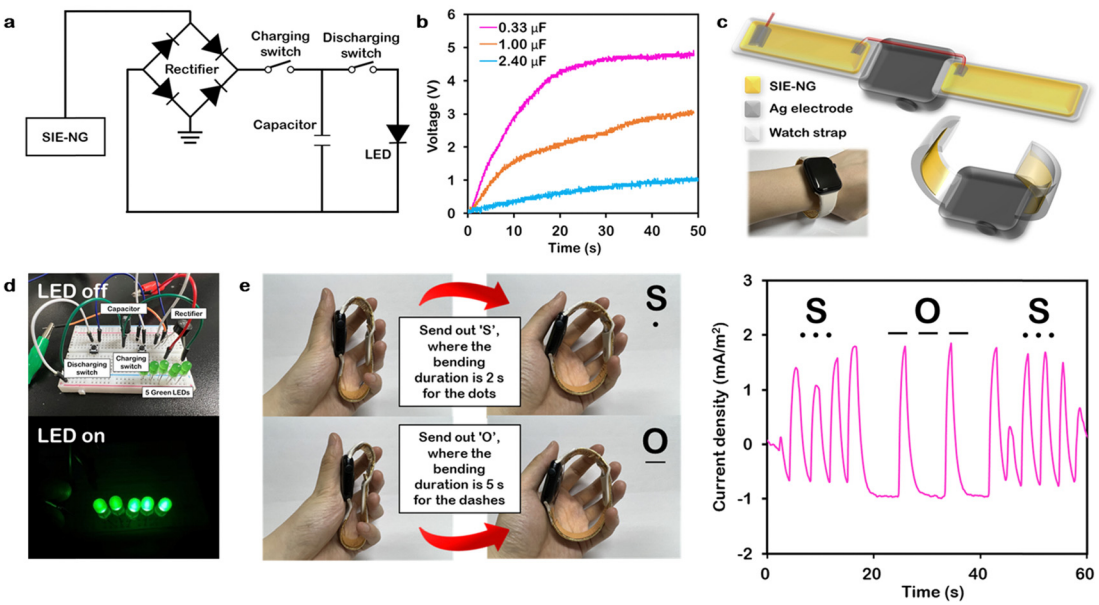

Fig. 5 Applications of the proposed SIE-NG: (a) schematic diagram illustrating the electrical circuit for energy storage. (b) Capacitor charging using 0.33. 1.00, and 2.40 μF capacitors (strain: 0.2%; frequency: 0.25 Hz). (c) Photograph showing the integration of SIE-NG into the watch strap. (d) Photograph of the five green LEDs powered by SIE-NG. (e) Photograph showing SIE-NG powering and generating an S.O.S. current signal in Morse code *via* finger grasping.

materials whose work functions can be modified by strain, further research and development efforts in this domain could catalyze transformative advancements and propel nanogenerator technology to unprecedented heights.

Author contributions

J. M. and S.-K. L. contributed equally to the work. J. M. conducted investigation process and data curation. S.-K. L. edited the script, conceived the experiments, and contributed to the establishment of a strain-induced electrification mechanism. B. I. performed the electrical performance evaluation. D. B. supported the financial for the project. D.-H. C. formulated overarching research aims and developed of methodology. D. B. and D.-H. C. revised the entire process and feedback the progress as corresponding authors. J. M., S.-K. L. and D.-H. C. wrote the manuscript. All authors reviewed the manuscript.

Data availability

The data supporting this article have been included as part of the ESI.†

Conflicts of interest

The authors declare no competing financial interests.

Acknowledgements

This research was supported by Basic Science Research Program through the National Research Foundation of Korea (NRF) funded by the Ministry of Education (RS-2023-00239590 and 2022R1F1A1072339), and the Technology Innovation Program funded by the Ministry of Trade, Industry, and Energy of Korea (Grant No. 20026376 (1415188205)).

References

1 Y. Su, G. Chen, C. Chen, Q. Gong, G. Xie, M. Yao, H. Tai, Y. Jiang and J. Chen, *Adv. Mater.*, 2021, **33**, 2101262.
2 S. Wang, L. Lin and Z. L. Wang, *Nano Energy*, 2015, **11**, 436–462.
3 S. P. Beeby, M. J. Tudor and N. White, *Meas. Sci. Technol.*, 2006, **17**, R175.
4 S. Roundy, *J. Intell. Mater. Syst. Struct.*, 2005, **16**, 809–823.
5 F.-R. Fan, Z.-Q. Tian and Z. L. Wang, *Nano Energy*, 2012, **1**, 328–334.
6 Z. L. Wang and J. Song, *Science*, 2006, **312**, 242–246.
7 Z. L. Wang, *Mater. Today*, 2017, **20**, 74–82.
8 R. Bechbache and J. Duffin, *J. Physiol.*, 1977, **272**, 553–561.
9 J. W. Hurst, *Circulation*, 1998, **98**, 1937–1942.
10 C. Liu, N. Zhang, J. Li, L. Dong, T. Wang, Z. Wang, G. Wang, X. Zhou and J. Zhang, *Nano Energy*, 2019, **65**, 104011.
11 I. V. Tikhonova, A. A. Grinevich and A. V. Tankanag, *Biomed. Signal Process. Control*, 2022, **71**, 103091.
12 G. Hotho, D. von Bonin, D. Krüerke, U. Wolf and D. Cysarz, *Front. Physiol.*, 2022, **13**, 875583.
13 J. Varghese, C. M. V. Alen, M. Fujarski, G. S. Schlake, J. Sucker, T. Warnecke and C. Thomas, *Sensors*, 2021, **21**, 3139.
14 M. Xu, T. Zhao, C. Wang, S. L. Zhang, Z. Li, X. Pan and Z. L. Wang, *ACS Nano*, 2019, **13**, 1932–1939.
15 A. Ahmed, I. Hassan, A. S. Helal, V. Sencadas, A. Radhi, C. K. Jeong and M. F. El-Kady, *Iscience*, 2020, **23**(7), 101286.
16 H. Jung, H. Ouro-Koura, A. Salalila, M. Salalila and Z. D. Deng, *Nano Energy*, 2022, **99**, 107365.
17 Y. Feng, X. Liang, J. An, T. Jiang and Z. L. Wang, *Nano Energy*, 2021, **81**, 105625.
18 Z. Bai, Y. Xu, C. Lee and J. Guo, *Adv. Funct. Mater.*, 2021, **31**, 2104365.
19 H. Dimigen and C.-P. Klages, *Surf. Coat. Technol.*, 1991, **49**, 543–547.
20 A. D. Moghadam, E. Omrani, P. L. Menezes and P. K. Rohatgi, *Composites, Part B*, 2015, **77**, 402–420.
21 Z. Zhao, X. Wang, Y. Hu, Z. Li, L. Li and G. Ye, *Tribol. Int.*, 2024, **191**, 109163.
22 J. Wu, Y. Xi and Y. Shi, *Nano Energy*, 2020, **72**, 104659.
23 S.-H. Chung, J. Chung and S. Lee, *Nanoenergy Adv.*, 2022, **2**, 210–221.
24 S. Wang, Y. Xie, S. Niu, L. Lin and Z. L. Wang, *Adv. Mater.*, 2014, **26**, 2818–2824.
25 K. Wang, Y. Zhang, X. Luo, L. Zhu and Z. L. Wang, *ACS Appl. Electron. Mater.*, 2022, **4**, 4764–4771.
26 M. Smetanin, D. Kramer, S. Mohanan, U. Herr and J. Weissmüller, *Phys. Chem. Chem. Phys.*, 2009, **11**, 9008–9012.
27 C. Xu, B. Zhang, A. C. Wang, W. Cai, Y. Zi, P. Feng and Z. L. Wang, *Adv. Funct. Mater.*, 2019, **29**, 1903142.
28 Y. Zi, C. Wu, W. Ding and Z. L. Wang, *Adv. Funct. Mater.*, 2017, **27**, 1700049.
29 X. Wang, W. Li, J. Lin and Y. Xiao, *Europhys. Lett.*, 2010, **89**, 66004.
30 A. M. Smith, A. M. Mohs and S. Nie, *Nat. Nanotechnol.*, 2009, **4**, 56–63.
31 W. Ma, *Phys. Status Solidi*, 2008, **245**, 761–768.
32 J.-H. Kim, A. Nizami, Y. Hwangbo, B. Jang, H.-J. Lee, C.-S. Woo, S. Hyun and T.-S. Kim, *Nat. Commun.*, 2013, **4**, 2520.
33 M. Haque and M. Saif, *Proc. Natl. Acad. Sci. U. S. A.*, 2004, **101**, 6335–6340.
34 S. Trasatti, *J. Electroanal. Chem. Interfacial Electrochem.*, 1974, **54**, 19–24.
35 Y. Umeno, C. Elsässer, B. Meyer, P. Gumbsch, M. Nothacker, J. Weißmüller and F. Evers, *Europhys. Lett.*, 2007, **78**, 13001.
36 B. Persson, *Tribol. Lett.*, 2023, **71**, 66.
37 Y. Xu, G. Min, N. Gadegaard, R. Dahiya and D. M. Mulvihill, *Nano Energy*, 2020, **76**, 105067.
38 B. Yang, W. Zeng, Z. H. Peng, S. R. Liu, K. Chen and X. M. Tao, *Adv. Energy Mater.*, 2016, **6**, 1600505.
39 J. Liu, N. Cui, T. Du, G. Li, S. Liu, Q. Xu, Z. Wang, L. Gu and Y. Qin, *Nanoscale Adv.*, 2020, **2**, 4482–4490.

40 F. Xing, Y. Jie, X. Cao, T. Li and N. Wang, *Nano Energy*, 2017, **42**, 138–142.
41 Y. Sun, L. Zhu, J. Yang, J. Zhang, B. Chen and Z. L. Wang, *Adv. Opt. Mater.*, 2022, **10**, 2101918.
42 Z. Qu, X. Wang, M. Huang, C. Chen, Y. An, W. Yin and X. Li, *Nano Energy*, 2023, **107**, 108094.
43 J. Xiong, P. Cui, X. Chen, J. Wang, K. Parida, M.-F. Lin and P. S. Lee, *Nat. Commun.*, 2018, **9**, 4280.
44 Z. Lin, B. Zhang, Y. Xie, Z. Wu, J. Yang and Z. L. Wang, *Adv. Funct. Mater.*, 2021, **31**, 2105237.
45 S. S. Kwak, S. M. Kim, H. Ryu, J. Kim, U. Khan, H.-J. Yoon, Y. H. Jeong and S.-W. Kim, *Energy Environ. Sci.*, 2019, **12**, 3156–3163.